

Original Paper

Palmitic Acid-Induced Podocyte Apoptosis via the Reactive Oxygen Species-Dependent Mitochondrial Pathway

Ting Liu^a Xue-mei Chen^b Ji-ye Sun^a Xu-shun Jiang^a Yue Wu^a Shan Yang^b
Hui-zhe Huang^c Xiong-zhong Ruan^{d,e} Xiao-gang Du^{a,f}

^aDepartment of Nephrology, The First Affiliated Hospital of Chongqing Medical University, Chongqing,

^bEmergency Department, The First Affiliated Hospital of Chongqing Medical University, Chongqing,

^cThe Second Affiliated Hospital of Chongqing Medical University, Chongqing, China, ^dCentre for Nephrology, Royal Free and University College Medical School, University College London, Royal Free Campus, London, United Kingdom, ^eCentre for Lipid Research, Key Laboratory of Molecular Biology on Infectious Diseases, Ministry of Education, Chongqing Medical University, Chongqing, ^fThe Chongqing Key Laboratory of Translational Medicine in Major Metabolic Disease, Chongqing, China

Key Words

Palmitic acid (PA) • Podocyte • Apoptosis • Reactive oxygen species (ROS) • Mitochondria

Abstract

Background/Aims: Chronic kidney disease (CKD) is often accompanied by hyperlipidemia, which accelerates progression of the disease. Podocyte injury can lead to dysfunction of the glomerular filtration barrier, which is associated with proteinuria, a risk marker for the progression of CKD. Our previous studies demonstrated that palmitic acid (PA) can induce podocyte apoptosis; however, the underlying mechanisms are unclear. In the present study, we investigated the specific molecular mechanisms of PA-induced apoptosis in cultured podocytes.

Methods: We cultured mouse podocytes and treated them with PA. Then, cell viability was measured using the Cell Counting Kit-8 colorimetric assay, lipid uptake was assessed by Oil Red O staining and boron-dipyrromethene staining, apoptosis was measured by flow cytometry, mitochondrial injury was assessed by JC-1 staining and transmission electron microscopy, and mitochondrial production of reactive oxygen species (ROS) was evaluated by fluorescence microscopy using the MitoSOX Red reagent. The effects of PA on the mitochondria-mediated caspase activation pathway were investigated by examining the expression of caspase-8, cleaved caspase-9, cleaved caspase-3, cleaved poly (ADP-ribose) polymerase (PARP), B-cell lymphoma 2 (Bcl-2), Bax, Bid, cytochrome *c*, and Fas-associated protein with death domain (FADD) using western blotting. The translocation of Bax and cytochrome *c* were detected by immunofluorescence. **Results:** PA treatment significantly increased lipid accumulation and induced podocyte apoptosis. We investigated whether the two primary apoptosis signaling

T. Liu and X. Chen contributed equally to this work.

Xiao-gang Du

Department of Nephrology, The First Affiliated Hospital of Chongqing Medical University
Youyi Road 1, Chongqing, 400042 (China)
Tel. +8613452058896, E-Mail cqmudxg@163.com

pathways (death receptor-mediated pathway and mitochondria-mediated pathway) were involved in the execution of PA-induced podocyte apoptosis, and found that the levels of FADD, caspase-8, and Bid did not significantly change during this process. Meanwhile, PA treatment induced an increase in Bax protein expression and a decrease in Bcl-2 protein expression, with Bax translocation to the mitochondria. Furthermore, PA treatment induced mitochondrial impairment, and triggered the release of cytochrome c from the mitochondria to cytosol, with a concomitant dose-dependent increase in the levels of cleaved caspase-9, cleaved caspase-3, and PARP. Meanwhile, PA treatment increased mitochondrial production of ROS, and the mitochondria-targeted antioxidant mitoTEMPO significantly ameliorated PA-induced podocyte apoptosis. **Conclusion:** Our findings indicated that PA induced caspase-dependent podocyte apoptosis through the mitochondrial pathway, and mitochondrial ROS production participated in this process, thus potentially contributing to podocyte injury.

© 2018 The Author(s)
Published by S. Karger AG, Basel

Introduction

Lipid disorders, mainly hypertriglyceridemia, are common in patients with all stages of chronic kidney disease (CKD) including diabetic nephropathy (DN) [1–4]. It has been reported that lipid abnormalities in renal disease contribute to the process of glomerulosclerosis with progressive renal dysfunction [5–9]. However, the mechanisms underlying how dyslipidemia accelerates CKD progression remain unclear.

Podocytes play a key role in glomerular selective filtration function [10, 11]. Podocyte dysfunction or injury induced by various stresses and pathological stimuli is thought to be critical for the pathogenesis of proteinuria and glomerular diseases [12, 13]. Podocytes are highly specialized and terminally differentiated visceral epithelial cells with a very limited ability to regenerate [14, 15]. Therefore, protecting them from injury and limiting their loss are important for the treatment of CKD. Podocyte apoptosis is one of the main risk factors causing podocyte loss [12, 16]. Our previous studies showed that palmitic acid (PA) can induce podocyte apoptosis [17, 18]. However, the precise mechanisms involved are not fully understood.

In this study, we aimed to elucidate the signaling pathway involved in PA-induced podocyte apoptosis.

Materials and Methods

Cell culture

The conditionally immortalized murine podocyte clone 5 (MPC5) cell line was a kind gift from Dr. Ruan (The Centre for Nephrology, Royal Free and University College Medical School, London, United Kingdom); they were cultured as previously described [17, 18]. Briefly, cells were cultured and maintained on type I collagen-coated dishes in RPMI-1640 medium (Gibco, Karlsruhe, Germany) supplemented with 10% fetal bovine serum (Gibco), 100 U/mL penicillin, and 100 µg/mL streptomycin at two different temperatures in a 5% CO₂ incubator. At 33°C (permissive condition), the cells were cultured in medium supplemented with 10 U/mL mouse recombinant interferon gamma (IFN-γ). To induce podocyte differentiation, the temperature was increased to 37°C (non-permissive condition) and cells were cultured in medium without IFN-γ for 14 days, after which subsequent experiments were performed.

Oil Red O staining and boron-dipyrromethene lipid probes

To observe fatty acid uptake by Oil Red O staining, the cells were fixed in 4% paraformaldehyde for 30 min, washed with phosphate-buffered saline (PBS), and incubated with Oil Red O working solution for 1 h. Then lipid droplets in podocytes were visualized by microscopy. To measure fatty acid uptake by boron-dipyrromethene (BODIPY) lipid probes, podocytes were incubated with 4, 4-difluoro-5-methyl-4-bora-3a,4a-diaza-s-indacene-3-dodecanoic acid (10 µg/mL, BODIPY 500/510 C1, C12; Invitrogen, Carlsbad,

CA, USA) for 1 h at 37°C, washed three times with PBS, and immediately visualized using a fluorescence microscope (DM4000; Leica, Wetzlar, Germany).

Cell death assessment

The effects of PA treatment on podocyte death were detected with a Cell Counting Kit-8 (CCK-8) colorimetric assay (Sigma-Aldrich, St. Louis, MO, USA). Briefly, podocytes were seeded at a density of 10^4 cells per well into 96-well plates and cultured in complete RPMI-1640 culture medium for 24 h. Then, the cells were treated with various concentrations of PA (0, 50, 150, and 300 μ M) for 24 h. CCK8 was added to each well, followed by a 2 h incubation at 37°C in a 5% CO₂ incubator. Absorbance was quantified by a multi-well fluorescence plate reader at 450 nm (Thermo Scientific Varioskan Flash; Thermo Fisher Scientific, Waltham, MA, USA). The cell death rate was calculated as follows: $(1 - A_{450} [\text{experimental}] / A_{450} [\text{control}]) \times 100\%$.

Flow cytometric analysis

Apoptosis was detected using the Annexin V-Fluorescein isothiocyanate (FITC)/propidium iodide (PI) apoptosis assay kit (Sungene Biotech, Tianjin, China). In brief, treated cells were collected by centrifugation, washed twice with ice-cold PBS, and resuspended in 500 μ L 1 \times Annexin V binding buffer containing 5 μ L Annexin V-FITC and 3 μ L of PI. After incubation for 10 min at room temperature, apoptosis was analyzed by flow cytometry.

Transmission electron microscopy

Treated podocytes were harvested and fixed in 2.5% glutaraldehyde for 24 h at 4°C, rinsed with PBS, and post-fixed in 1% osmium tetroxide and 0.1% potassium ferricyanide. After rinsing with 0.1 M cacodylate buffer, the samples were dehydrated through a graded series of ethanol (30–90%) washes and embedded in a mixture of epoxy resin. Sections were cut using a diamond knife on an ultramicrotome (ULTRACUT E; Reichert-Jung, Vienna, Austria) and stained with 1% uranyl acetate and Reynolds lead citrate. The sections were examined using a JEM-1200 EXII transmission electron microscope (JEOL, Tokyo, Japan).

Measurement of mitochondrial reactive oxygen species production

Mitochondrial superoxide production was measured with MitoSOX Molecular Probes (M36008; Invitrogen), a red fluorescent dye that localizes to mitochondria. Treated cells were washed twice with PBS and then incubated with MitoTracker Green (C1048; Beyotime, Jiangsu, China) and MitoSOX for 30 min at 37°C. Cell fluorescence was observed by fluorescence microscopy at wavelengths of 488 nm for excitation and 525 nm for emission.

Assays for mitochondrial membrane potential

The mitochondrial membrane potential ($\Delta\Psi_m$) of podocytes was detected using a mitochondrial membrane potential assay kit (JC-1; Beyotime). In accordance with the manufacturer's instructions, differentiated podocytes were grown on a glass coverslip in 12-well culture plates, pretreated with PA (150 μ M) for 24 h, and incubated with JC-1 (300 nM) at 37°C for 20 min. Images were captured using a fluorescence microscope. Mitochondrial uncoupler carbonyl cyanide *m*-chlorophenylhydrazone (CCCP) was used as a positive control.

Mitochondrial morphology examined by fluorescence microscopy

Differentiated podocytes cultured on confocal dishes were treated with 150 μ M PA for 24 h and then stained with MitoTracker Deep Red (M22426; Invitrogen) for 30 min at 37°C. Fluorescence images for MitoTracker (excitation/emission: 644/665 nm) were obtained using a confocal microscope (A1R; Nikon, Tokyo, Japan).

Immunocytochemistry

Podocytes cultured on coverslips were washed three times with PBS, stained with or without MitoTracker Deep Red at 37°C for 30 min, fixed in 4% paraformaldehyde for 30 min, permeabilized with 0.1% Triton X-100 for 15 min, and blocked with 5% bovine serum albumin (BSA) for 1 h at room temperature. The cells were incubated with different antibodies (rabbit anti-Bax, 1:200; Cell Signaling Technology

[CST], Danvers, MA, USA and rabbit anti-cytochrome *c*, 1:100; Abcam, Cambridge, UK) overnight at 4°C, followed by incubation with an Alexa Fluor 546 donkey anti-rabbit IgG (1:400, A10040; Invitrogen) for 1 h at 37°C. The cells were washed and counterstained with 10 ng/mL DAPI for 3 min. Fluorescence images were observed using a confocal microscope. Quantification of all immunofluorescence data was performed in individual frames after deconvolution and thresholding using Image J software (National Institutes of Health, Bethesda, MD, USA). Specifically, quantification of the target protein was based on at least three fields taken at random from each slide. The area ratio between the target protein and cells in every field was calculated (with content color thresholds). Then the area ratio was normalized to the control group. To show colocalization, Image J was used to measure the gray value within lines drawn in the images (with content Plot Profile). Then line graphs were completed in GraphPad.

Western blot analysis

After treatments, cells were washed with ice-cold PBS, lysed with ice-cold RIPA buffer (Beyotime) containing protease inhibitors, sonicated (noise-isolating tamber, Ningbo Scientz Biotechnology Co., Ltd.) for 12 s (20% power, 1-s pulse on, 2-s pulse off), and centrifuged at 12,000 g for 20 min at 4°C. Protein concentrations were determined with the BCA Protein Assay Kit (Beyotime). Equal amounts of protein samples were loaded per lane, separated by sodium dodecyl sulfate-polyacrylamide gel electrophoresis, and electrophoretically transferred onto polyvinylidene fluoride membranes (Millipore, Stafford, VA, USA). The membranes were blocked in 5% skim milk for 3 h. Then the PVDF membranes were incubated with different primary antibodies: rabbit anti-caspase-8 (1:1000; CST), mouse anti-cleaved caspase-9 (1:1000; CST), rabbit anti-cleaved caspase-3 (1:1000; CST), rabbit anti-poly (ADP-ribose) polymerase (PARP) (1:1000; CST), rabbit anti-B-cell lymphoma 2 (Bcl-2) (1:1000; CST), rabbit anti-Bax (1:1000; CST), rabbit anti-Bid (1:1000; CST), rabbit anti-cytochrome *c* (1:2000; Abcam), rabbit anti-Fas-associated protein with death domain (FADD) (1:2000; Abcam), and mouse anti- β -actin (1:5000; Sungene Biotech) overnight at 4°C, followed by incubation with horseradish peroxidase-conjugated secondary antibodies for 1 h at room temperature. The signals were detected using an ECL chemiluminescence system (GE Healthcare, Piscataway, NJ, USA), the band intensities were quantified with Quantity One software, and the results were normalized to those of β -actin.

Statistical analysis

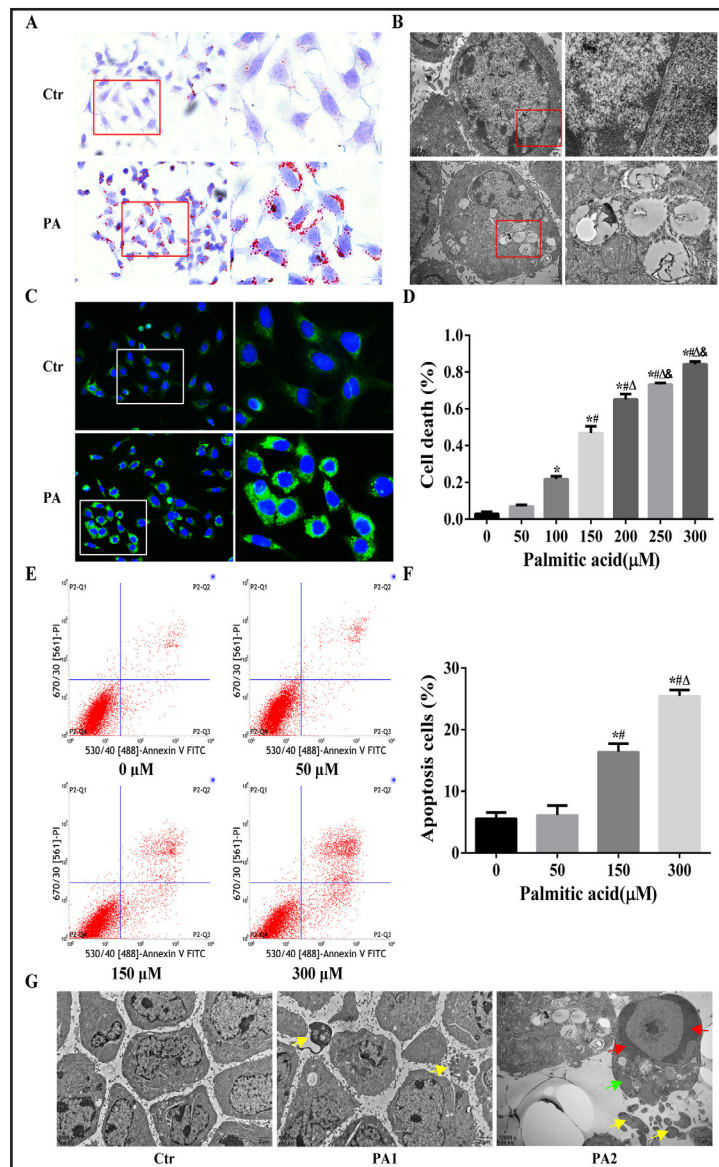
The data are shown as the mean \pm standard error of the mean of three independent experiments performed in triplicate. Statistical analyses were performed using GraphPad Prism 6.0 (GraphPad software, San Diego, CA, USA). Statistical comparisons between the two groups were analyzed using the two-tailed unpaired Student's *t*-test, and multiple comparisons were performed using one-way analysis of variance followed by Tukey's *t*-test. A value of $P < 0.05$ was defined as statistically significant.

Results

PA induced lipid accumulation, cell death, and cell apoptosis in podocytes

Using Oil Red O staining, BODIPY lipid probes, and transmission electron microscopy (TEM), we found that exposing podocytes to 150 μ M PA induced obvious intracellular lipid accumulation and lipid droplet formation compared with the control cells (Fig. 1A, 1B, and 1C). To evaluate the effects of PA on cell death, the CCK-8 assay was conducted. After 24 h of incubation with different concentrations of PA, we observed a concentration-dependent increase in cell death (Fig. 1D). Apoptosis is one of the main types of cell death and plays a fundamental role in the development of multicellular organisms [19]. We measured apoptosis using Annexin V-FITC/PI staining and flow cytometry, and found that PA dose-dependently induced podocyte apoptosis (Fig. 1E and 1F). Next, we observed the subcellular changes of podocytes by TEM, and found that PA-induced podocytes showed obvious apoptotic features such as chromatin peripheralization, cytoplasm condensation, and breakdown and formation of apoptotic bodies consisting of cytoplasm and tightly packed organelles with or without nuclear fragments within an intact plasma membrane (Fig. 1G).

Fig. 1. Palmitic acid induced lipid accumulation, cell death, and cell apoptosis in podocytes. Differentiated podocytes cultured on coverslips were treated with 150 μM palmitic acid (PA) for 24 h, after which the lipid content was evaluated by (A) Oil Red O staining (400 \times), (B) transmission electron microscopy (TEM) (12, 000 \times), (C) and BODIPY lipid probes (400 \times). The rightmost panels show enlarged views of the boxed areas in Fig. 1A, 1B, and 1C. (D-F) Podocytes were treated with different concentrations of PA for 24 h. (D) Cell death was evaluated by the CCK-8 assay. The data are shown as the mean \pm standard error of the mean (SEM), $n = 3$. *, $P < 0.05$ vs. control group; #, $P < 0.05$ vs. 50 μM group; Δ , $P < 0.05$ vs. 100 μM group; &, $P < 0.05$ vs. 150 μM group. (E-F) Apoptosis was detected by flow cytometry. (E) Representative cytograms of apoptosis. (F) Quantification of cell apoptosis. The data are shown as the mean \pm SEM, $n = 3$. *, $P < 0.05$ vs. control group; #, $P < 0.05$ vs. 50 μM group; Δ , $P < 0.05$ vs. 150 μM group. (G) Apoptosis were detected by TEM. Panel Ctr and panel PA1 are 5000 \times magnification, panel PA2 is 12, 000 \times magnification. PA-treated podocytes showed obvious apoptotic features such as chromatin peripheralization (red arrow), cytoplasm condensation (green arrow), and breakdown and formation of apoptotic bodies consisting of cytoplasm and tightly packed organelles with or without nuclear fragments within an intact plasma membrane (yellow arrow). Ctr: control group, podocytes were treated with 1% defatted-BSA; PA1 and PA2: palmitic acid group, podocytes were treated with 150 μM palmitic acid for 24 h.



PA-induced podocyte apoptosis was independent of the death receptor pathway

There are two predominant signaling pathways that trigger apoptotic cell death: the death receptor (extrinsic) pathway and the mitochondrial (intrinsic) pathway [19–21]. Upon stimulation, FADD, an apoptotic adaptor molecule, recruits caspase-8 to the activated Fas (CD95) receptors to form the death-inducing signaling complex. Then, activated caspase-8 initiates the caspase cascade, ultimately leading to apoptosis. This is termed the death receptor pathway [19]. Furthermore, activated caspase-8 can cleave Bid (a BH3-only pro-apoptotic protein, which is thought to be a bridging element between the death receptor pathway and mitochondrial pathway) to produce truncated Bid (tBid), which promotes

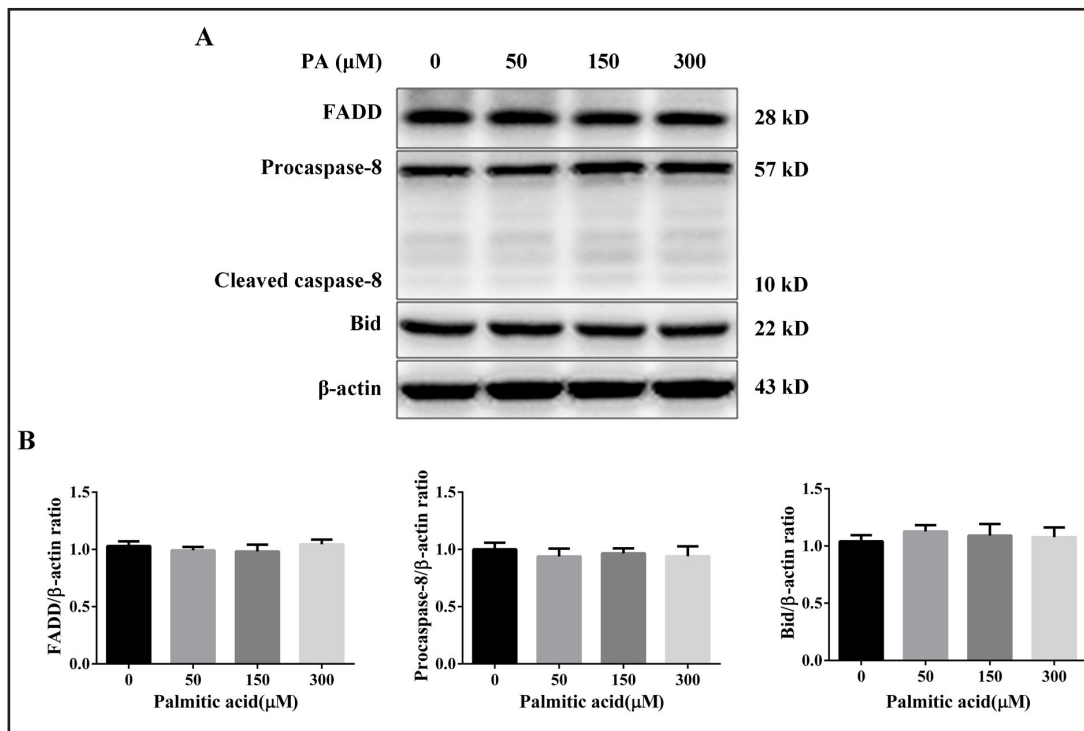


Fig. 2. Podocyte apoptosis induced by PA was independent of the death receptor pathway. (A) Podocytes were treated with different concentrations of PA for 24 h. Representative bands of Fas-associated protein with death domain (FADD), caspase-8, and Bid protein expression were detected by western blotting. β-actin was used as a loading control. (B) Densitometric analysis of FADD, caspase-8, and Bid expression in Fig. 2A. The statistical data are presented as the mean ± SEM from three independent experiments. *, P<0.05 vs. control group; #, P<0.05 vs. 50 μM group; Δ, P<0.05 vs. 150 μM group.

the translocation of Bax from the cytosol to the mitochondria and subsequent activation of the mitochondrial pathway [22]. In this study, no significant difference in the expression of FADD, caspase-8, and Bid was found between the PA-treated group and control group (Fig. 2A and 2B), indicating that PA induced podocyte apoptosis independently of the death receptor pathway.

PA increased the Bax/Bcl-2 ratio and induced Bax translocation to the mitochondria in podocytes

The Bcl-2 family of proteins, which contain Bcl-2 homology (BH) domains, consist of pro-apoptotic members including Bax and anti-apoptotic members including Bcl-2. The imbalance between pro-apoptotic and anti-apoptotic members of the Bcl-2 family determines the ultimate fate of cells [23]. In this study, we observed that PA induced an increase in Bax expression and decrease in Bcl-2 expression in a dose-dependent manner in podocytes (Fig. 3A, B). Next, we investigated the location of Bax in PA-treated podocytes and found that Bax staining (green) mainly located outside the mitochondria (red) in control cells, whereas in PA-treated cells, the green fluorescence of Bax mainly co-localized with the red fluorescence of the mitochondria, as shown by the orange staining of the mitochondria in the merged image, indicating that PA induced Bax translocation from the cytosol to the mitochondria in podocytes (Fig. 3C, 3D, and 3E).

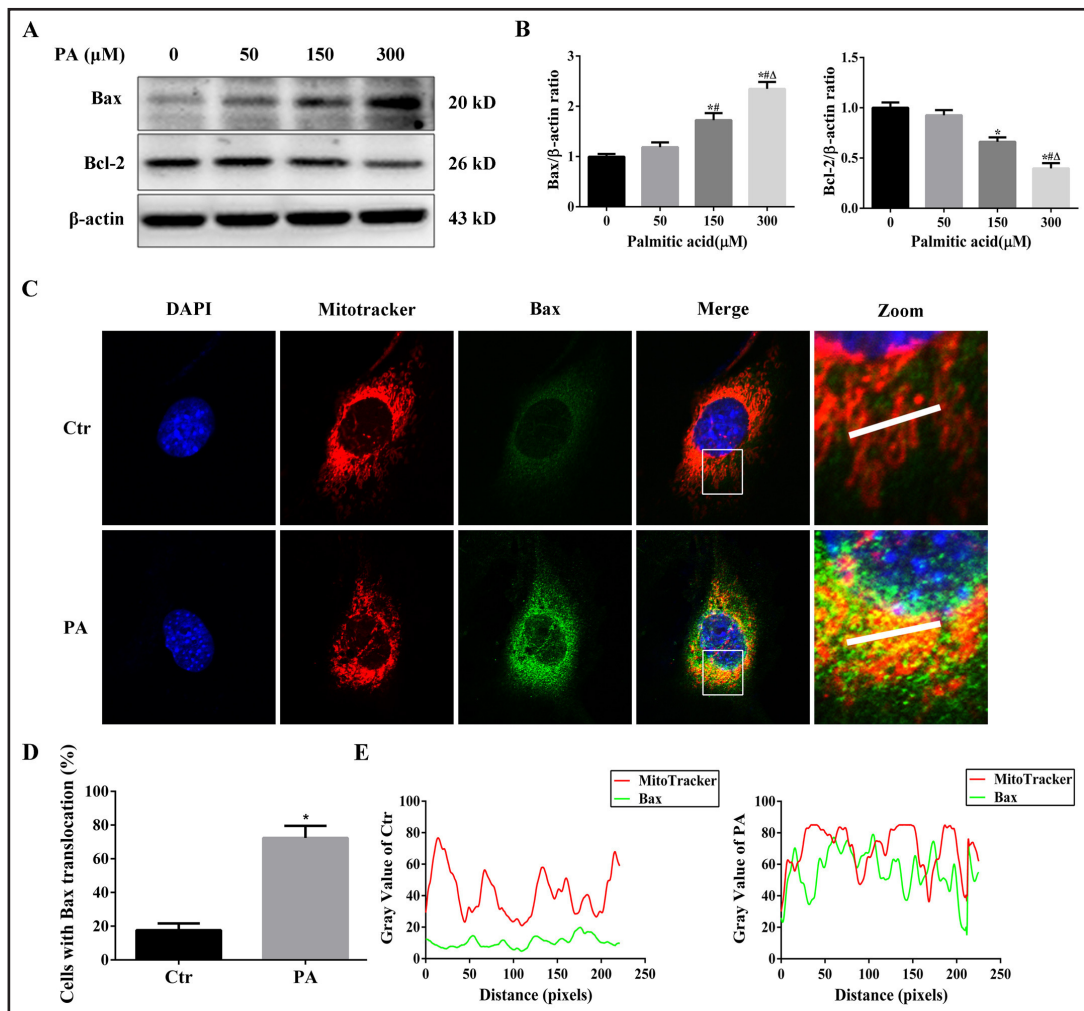


Fig. 3. PA induced increased Bax and reduced Bcl-2 protein expression, and Bax translocation to the mitochondria of podocytes. (A) Podocytes were treated with different concentrations of PA for 24 h. Representative bands of Bax and Bcl-2 protein expression were detected by western blotting. β-actin was used as a loading control. (B) Densitometric analysis of Bax and Bcl-2 expression in Fig. 3A. The statistical data are presented as the mean ± SEM from three independent experiments. *, P<0.05 vs. control group; #, P<0.05 vs. 50 μM group; Δ, P<0.05 vs. 150 μM group. (C) Mitochondria was stained by MitoTracker Deep Red and then stained with an antibody against Bax. Representative images of the cells were taken with a confocal microscope (1200×). The rightmost panels showed enlarged views of the boxed areas in the left panels. (D) Quantification of Bax translocation to the mitochondria in PA-treated cells. The localization of Bax in MitoTracker-stained cells was evaluated to determine the percentage of cells that showed Bax accumulation in mitochondria. The data represent three independent experiments with at least 50 cells scored from several random fields. The statistical data are presented as the mean ± SEM from three independent experiments, *, P<0.05 vs. control group. (E) Line scans indicate co-localizations between Bax (Green) and MitoTracker (Red) and correlate to the lines drawn in the images. Ctr: control group, podocytes were treated with 1% defatted-BSA; PA: palmitic acid group, podocytes were treated with 150 μM PA for 24 h.

PA induced podocyte apoptosis through activation of the mitochondrial pathway

As mitochondrial membrane integrity is regulated by Bcl-2 protein family members such as Bcl-2 (anti-apoptotic) and Bax (pro-apoptotic) [22, 23], we further investigated the change of ΔΨ_m using the fluorescent probe JC-1 and found a large accumulation of J-aggregates

(red fluorescence) and a small population of J-monomers (green fluorescence) in the control group. However, PA-treated cells and $\Delta\Psi_m$ disrupter CCCP-treated cells showed more diffuse J-monomer fluorescence and less apparent accumulation of J-aggregates in (Fig. 4A and 4C), which indicated that PA induced depolarization in the $\Delta\Psi_m$ of podocytes, which is a distinctive feature of early-stage apoptosis. Normal $\Delta\Psi_m$ is required to sustain mitochondrial morphology and structure. We observed mitochondrial morphology changes using confocal microscopy and found interconnected and rod-shaped mitochondria in untreated podocytes, but dot-like round and fragmented mitochondria in PA-treated podocytes (Fig. 4E). TEM images also showed abnormal mitochondria including mitochondrial enlargement and swelling with cristae loss and inner membrane destruction in PA-treated podocytes (Fig. 4F and 4G). Mitochondrial depolarization triggers mitochondrial outer membrane permeabilization, facilitating the release of cytochrome *c* from dysfunctional mitochondria into the cytoplasm, which leads to activation of the caspase cascade (apoptotic markers) and mitochondria-mediated apoptosis [24]. In present study, we observed that PA treatment significantly increased the expression of cytochrome *c* in a dose-dependent manner, as determined by western blot analysis (Fig. 4B and 4D). Meanwhile, we found that in control cells, cytochrome *c* staining (green) mainly co-localized with the mitochondria (red), as shown by the orange staining of the mitochondria in the merged image. Nevertheless, the diffuse green staining of cytochrome *c* mainly located outside the mitochondria (red) in PA-treated cells (Fig. 4H–J). All of these data indicated that PA induced the release of cytochrome *c* from the mitochondria into the cytosol of podocytes. Caspases are the central components in the execution of apoptosis. In general, they are involved in apoptosis and are divided into initiator and executioner caspases. Caspase-9 is the initiator caspase in the mitochondrial pathway. Caspase-3, which is downstream of caspase-9, is the key executioner caspase in apoptosis [25, 26]. Using western blot analysis, we found that PA treatment significantly induced activation of caspase-9 and caspase-3 in a dose-dependent manner (Fig. 4K and 4L). At the same time, exposure of podocytes to PA also resulted in PARP cleavage (Fig. 4K and 4L), which is an endogenous substrate of activated caspase-3, its cleavage is considered a hallmark of apoptosis. These results indicated that PA treatment induced apoptosis in podocytes via activation of the mitochondrial (intrinsic) apoptotic pathway.

Role of mitochondrial ROS production in PA-induced podocyte apoptosis

ROS is a collective term for various short-lived oxygen-containing molecules that are highly reactive and can promote oxidative stress [27]. They are the byproducts of aerobic respiration, and primarily arise from the mitochondria; excessive ROS production can cause damage to the mitochondria [28, 29]. In this study, we found that PA promoted mitochondrial ROS production in podocytes by using the MitoSOX molecular probe (Fig. 5A and 5C). The mitochondrial apoptotic pathway is involved in oxidative stress-induced cell apoptosis [30–32]. To verify the role of PA-induced mitochondrial ROS production in the mitochondrial apoptotic pathway, differentiated podocytes were pre-incubated with the mitochondrial antioxidant, mitoTEMPO (100 nM) for 1 h and then treated with PA (150 μ M) for 24 h. As shown in Fig. 5A and 5C, pretreatment with mitoTEMPO significantly attenuated PA-induced mitochondrial ROS accumulation in podocytes. In addition, PA-induced podocyte apoptosis was significantly ameliorated by pretreatment with mitoTEMPO (Fig. 5B, 5D, 5E, and 5F). These data support our hypothesis that oxidative stress originating from the mitochondria is involved in PA-induced apoptosis in podocytes. Taken together, these data strongly demonstrate that the mitochondrial apoptotic pathway is involved in the execution of apoptosis in PA-treated podocytes, and mitochondrial ROS production takes part in PA-induced podocyte apoptosis.

Fig. 4. PA induced podocyte apoptosis through the mitochondrial pathway. (A) Podocytes were treated with 150 μ M PA for 24 h or 10 μ M carbonyl cyanide m-chlorophenylhydrazone (CCCP) for 1 h. The JC-1 red/green fluorescence ratio reflects the mitochondrial membrane potential (400 \times). (B) Representative bands of cytochrome c protein expression were detected by western blot analysis. β -actin was used as a loading control. (C) Fluorescence intensities from five randomly selected microscopic fields per group in Fig. 4A were measured and analyzed. The statistical data are presented as the mean \pm SEM from three independent experiments. *, P<0.05 vs. control group. (D) Densitometric analysis of cytochrome c expression in Fig. 4B. The statistical data are presented as the mean \pm SEM from three independent experiments. *, P<0.05 vs. control group; #, P<0.05 vs. 50 μ M group; Δ , P<0.05 vs. 150 μ M group. (E, F) Representative images of mitochondrial morphology. (E) Podocytes were stained with MitoTracker Deep Red and then examined under a confocal microscope (1200 \times). (F) Structural alterations of mitochondria were analyzed by transmission electron microscopy (30,000 \times). (G) Mitochondrial injury in Fig. 4F was calculated and expressed as a percentage of damaged mitochondria over the total number of mitochondria counted under three different sections. Data are expressed as the mean \pm SEM from three independent experiments. *, P<0.05 vs. control group. (H) Mitochondria was stained by MitoTracker Deep Red and then stained with an antibody against cytochrome c. Representative images of the cells were taken with a confocal microscope (1200 \times). The rightmost panels showed enlarged views of the boxed areas in the left panels in Fig. 4E, 4F, and 4H. (I) Quantification of cytochrome c release into the cytosol of PA-treated cells. The localization of cytochrome c in MitoTracker-stained cells was evaluated to determine the percentage of cells that released cytochrome c into cytosol. The data represent three independent experiments with at least 50 cells scored from several random fields. The statistical data are presented as the mean \pm SEM from three independent experiments, *, P<0.05 vs. control group. (J) Line scans indicate co-localizations between cytochrome c (Green) and MitoTracker (Red) and correlate to the lines drawn in the images. (K) Representative bands of cleaved caspase-9, PARP and cleaved caspase-3 protein expression were detected by western blot analysis. β -actin was used as a loading control. (L) Densitometric analysis of cleaved caspase-9, PARP, and cleaved caspase-3 expression in Fig. 4K. The statistical data are presented as the mean \pm SEM from three independent experiments. *, P<0.05 vs. control group; #, P<0.05 vs. 50 μ M group; Δ , P<0.05 vs. 150 μ M group. Ctr: control group, podocytes were treated with 1% defatted-BSA; PA: palmitic acid group, podocytes were treated with 150 μ M PA for 24 h.

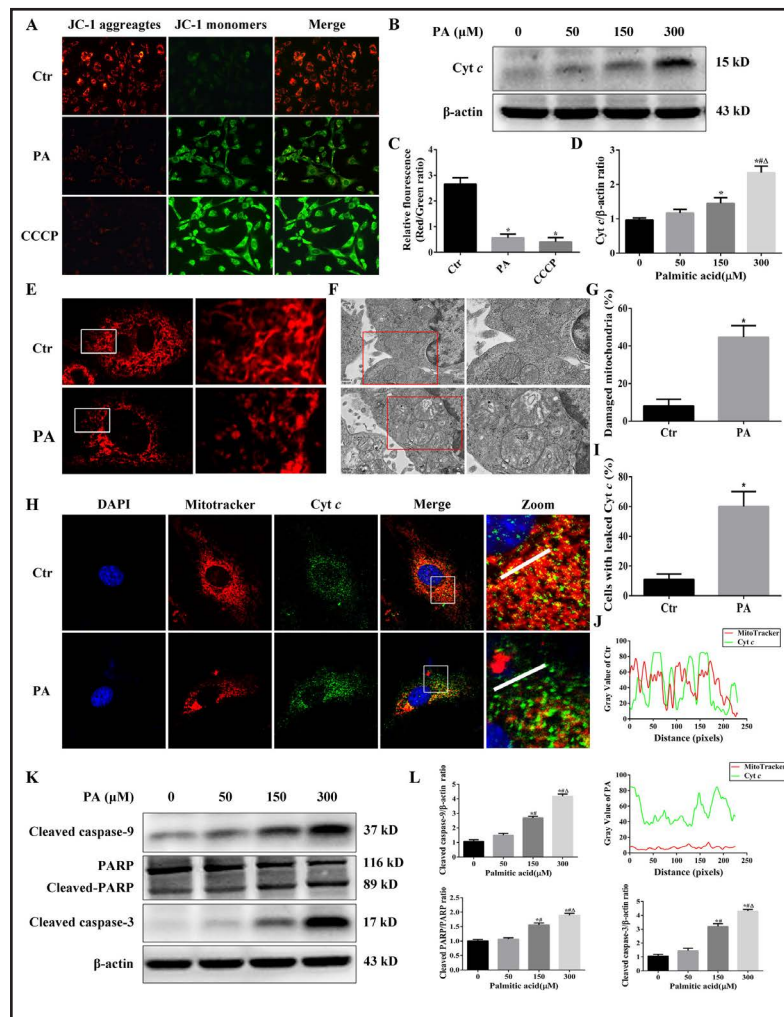
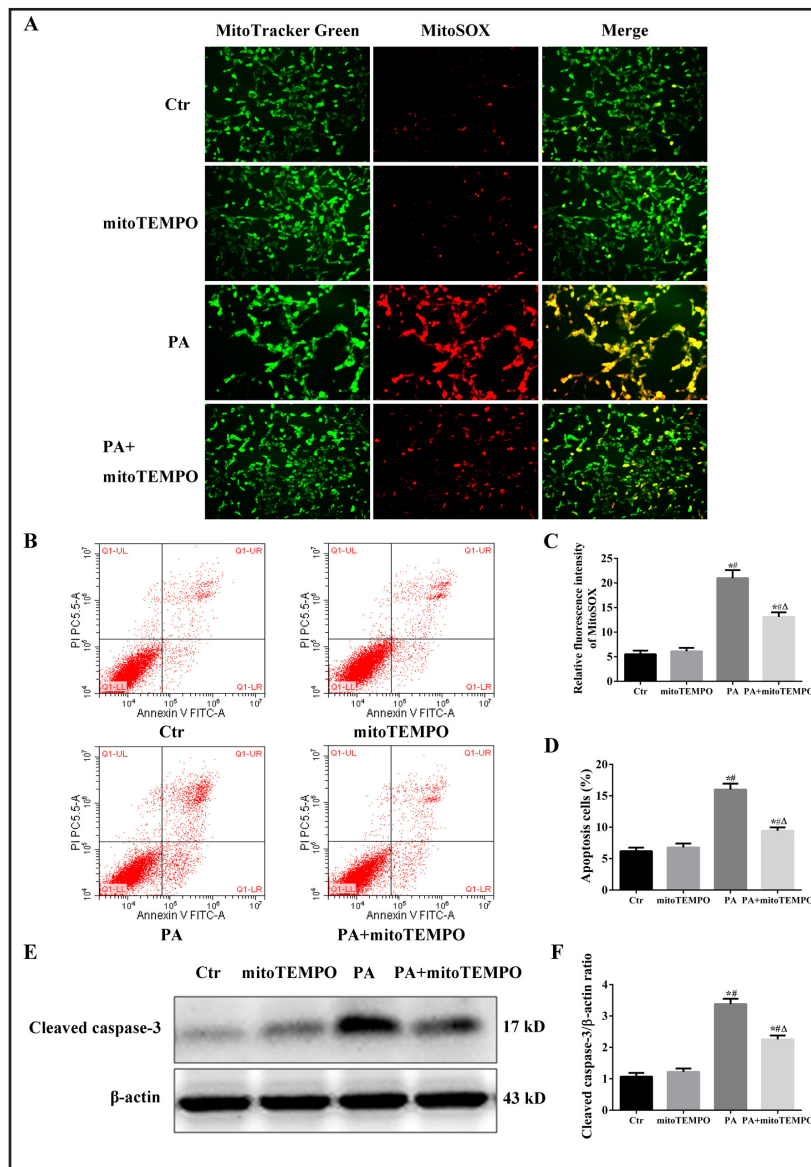


Fig. 5. Role of mitochondrial ROS production in PA-induced podocyte apoptosis. Differentiated podocytes were treated with PA (150 μ M) for 24 h in the presence or absence of preincubation with mitoTEMPO (100 nM) for 1 h. (A) Mitochondrial ROS were labeled with MitoSOX (200 \times). Fluorescence was visualized using a fluorescence microscope. (B) Flow cytometric analysis of cell apoptosis was conducted using Annexin V-FITC+PI staining. (C) Relative fluorescence intensities of mitoSOX from three randomly selected microscopic fields per group were measured and analyzed. (D) Percentage of apoptotic cells. (E) Western blot analysis of the protein level of cleaved caspase-3. β -actin was used as a loading control. (F) Densitometric analysis of cleaved caspase-3 expression in Fig. 5E. Statistical data are presented as the mean \pm SEM from three independent experiments. *, $P < 0.05$ vs. control group; #, $P < 0.05$ vs. mitoTEMPO group; Δ , $P < 0.05$ vs. PA group. Ctr: control group, podocytes were treated with 1% defatted-BSA; mitoTEMPO: podocytes were treated with 1% defatted-BSA for 24 h after pretreatment with 100 nM mitoTEMPO for 1 h; PA: palmitic acid group, podocytes were treated with 150 μ M PA for 24 h; PA+ mitoTEMPO: podocytes were treated with 150 μ M PA for 24 h after pretreatment with 100 nM mitoTEMPO for 1 h.



Discussion

CKD is often accompanied by hyperlipidemia, which is associated with accelerated CKD progression [3, 5, 33]. Podocytes form an important cellular layer of the glomerular filtration barrier, which is involved in the regulation of glomerular permselectivity [34]. Podocyte injury or dysfunction plays a pivotal role in the development of proteinuria in all forms of glomerular nephritis and DN [35, 36]. Hence, maintaining the structural and functional integrity of podocytes and protecting podocytes from injury have become potential therapeutic approaches for CKD. However, the exact mechanisms involved are still unclear.

In this study, we treated MPC5 cells with PA to create an *in vitro* hyperlipidemia model, and found that PA could increase lipid accumulation, and induce cell death and apoptosis in podocytes.

The mechanism of podocyte apoptosis is complex. It has been reported that palmitate can induce podocyte apoptosis by activating the endoplasmic reticulum (ER) stress-mediated apoptotic pathway [37–41]; however, it remains unknown whether the two primary apoptosis signaling pathways (death receptor-mediated pathway and mitochondria-mediated pathway) are also involved in the execution of PA-induced podocyte apoptosis. The death receptor-mediated pathway is an extrinsic signaling pathway that is activated upon ligation of cell surface death receptors, including Fas, the TRAIL receptor, and tumor necrosis factor receptor [42], and recruits the adapter protein FADD and procaspase-8 to form the death-inducing signaling complex (DISC). This protein complex serves as a platform for caspase activation, and the auto-catalytic activation of caspase-8 at the DISC leads to activation of caspase-3, triggering the apoptotic process [43, 44]. In this study, we found that the levels of FADD, caspase-8, and Bid did not significantly change during the process of PA-induced podocyte apoptosis. Mitochondria-mediated pathway of apoptosis is the intrinsic pathway, which is triggered upon mitochondrial injury including loss of integrity of mitochondrial outer membrane. Then, cytochrome *c* is released from the mitochondria into the cytosol. The Bcl-2 protein family controls this process. Once in the cytosol, cytochrome *c* recruits procaspase-9 to the apoptosome, which induces cleavage of downstream effector caspase-3, resulting in apoptosis [45–47]. Here, we found that PA treatment resulted in the increased expression of Bax/Bcl-2, depolarization of $\Delta\Psi_m$, mitochondrial swelling and destruction, and release of cytochrome *c* from the mitochondria into the cytosol of podocytes. These perturbations, in turn, activate caspase cascades (caspase-9 and caspase-3) in a dose-dependent manner. PARP, a marker of caspase-3 activation during apoptosis [48], was also clearly cleaved after PA treatment in podocytes. This finding indicates that the mitochondria-mediated apoptotic pathway, rather than the death receptor pathway, is involved in the process of PA-induced apoptosis in podocytes.

ROS, the products of normal metabolism and xenobiotic exposure, can be beneficial or harmful to cells and tissues. Mounting evidence suggests that moderate levels of ROS are beneficial for cell proliferation and differentiation [49], whereas excessive ROS can cause protein oxidation, lipid peroxidation, and DNA damage, thus leading to cell damage and apoptosis [47, 50, 51]. Mitochondria are both the major source of intracellular ROS production and targets of ROS [52]. Here, we found that PA accelerated mitochondrial ROS production and apoptotic cell death in podocytes, and the mitochondrial antioxidant mitoTEMPO ameliorated PA-induced podocyte apoptosis, which indicated that oxidative stress originating from the mitochondria mediated PA-induced podocyte apoptosis.

In this study, we showed that in addition to the ER stress-induced apoptotic pathway, the intrinsic mitochondrial apoptotic pathway in podocytes can also be activated by PA. However, the relationship between these two apoptotic pathways in PA-induced podocytes is still uncertain and is the subject of ongoing investigations.

Conclusion

We demonstrated that PA induces lipid accumulation, mitochondrial injury, and apoptosis in podocytes. The mitochondria-mediated apoptotic pathway, rather than the death receptor pathway, is the main pathway involved in PA-induced apoptosis in podocytes, and excessive ROS production derived from damaged mitochondria is a key underlying mechanism. Further studies are required to determine the relationship between the mitochondria-mediated apoptotic and ER stress-mediated apoptotic pathways, and how they are regulated in podocytes in high lipid conditions.

Disclosure Statement

The authors have no conflicts of interest to disclose.

Acknowledgements

This work was supported by a grant from the National Natural Science Foundation of China (No. 81370816), grants from the Natural Science Foundation of Chongqing Science and Technology Commission of China (No. cstc2012jjA10136) and the Chongqing Municipal Health Bureau of China (No. 2011-1-016) to X. Du, a grant from the National Natural Science Foundation of China (No. 31171619) and a grant from the Natural Science Foundation of Chongqing Science and Technology Commission of China (No. cstc2012jjq10001) to H. Huang.

XMC and XGD conceived and designed the experiments. TL and XMC performed the experiments. TL, XMC, and XGD analyzed the results. JYS, XSJ, YW, SY, HZH, and XZR contributed reagents, materials, and analytical tools. TL, XMC, and XGD wrote the manuscript.

References

- 1 Senti M, Romero R, Pedro-Botet J, Pelegri A, Nogues X, Rubies-Prat J: Lipoprotein abnormalities in hyperlipidemic and normolipidemic men on hemodialysis with chronic renal failure. *Kidney Int* 1992;41:1394-1399.
- 2 Attman P-O, Samuelsson O, Alaupovic P: Lipoprotein Metabolism and Renal Failure. *Am J Kidney Dis* 1993;21:573-592.
- 3 Kwan BC, Kronenberg F, Beddhu S, Cheung AK: Lipoprotein metabolism and lipid management in chronic kidney disease. *J Am Soc Nephrol* 2007;18:1246-1261.
- 4 Arnadottir M, Thysell H, Dallongeville J, Fruchart JC, Nilsson-Ehle P: Evidence that reduced lipoprotein lipase activity is not a primary pathogenetic factor for hypertriglyceridemia in renal failure. *Kidney Int* 1995;48:779-784.
- 5 Wheeler DC, Bernard DB: Lipid Abnormalities in the Nephrotic Syndrome: Causes, Consequences, and Treatment. *Am J Kidney Dis* 1994;23:331-346.
- 6 Kees-Folts D, Diamond JR: Relationship between hyperlipidemia, lipid mediators, and progressive glomerulosclerosis in the nephrotic syndrome. *Am J Nephrol* 1993;13:365-375.
- 7 Thabet MA, Salcedo JR, Chan JC: Hyperlipidemia in childhood nephrotic syndrome. *Pediatr Nephrol* 1993;7:559-566.
- 8 Srivastava SP, Shi S, Koya D, Kanasaki K: Lipid mediators in diabetic nephropathy. *Fibrogenesis Tissue Repair* 2014;7:12.
- 9 Yukawa S, Mune M, Yamada Y, Otani H, Kishino M, Tone Y: Ongoing clinical trials of lipid reduction therapy in patients with renal disease. *Kidney Int Suppl* 1999;71:S141-143.
- 10 Brinkkoetter PT, Ising C, Benzing T: The role of the podocyte in albumin filtration. *Nat Rev Nephrol* 2013;9:328-336.
- 11 Zhang H, Ren R, Du J, Sun T, Wang P, Kang P: AF1q Contributes to Adriamycin-Induced Podocyte Injury by Activating Wnt/beta-Catenin Signaling. *Kidney Blood Press Res* 2017;42:794-803.
- 12 Mundel P: Podocyte Biology and Response to Injury. *J Am Soc Nephrol* 2002;13:3005-3015.
- 13 Greka A, Mundel P: Cell biology and pathology of podocytes. *Annu Rev Physiol* 2012;74:299-323.
- 14 Hagen M, Pfister E, Kosel A, Shankland S, Pippin J, Amann K, Daniel C: Cell cycle re-entry sensitizes podocytes to injury induced death. *Cell Cycle* 2016;15:1929-1937.
- 15 Abu Hamad R, Berman S, Hachmo Y, Stark M, Hasan F, Doenyas-Barak K, Efrati S: Response of Renal Podocytes to Excessive Hydrostatic Pressure: a Pathophysiologic Cascade in a Malignant Hypertension Model. *Kidney Blood Press Res* 2017. DOI: 10.1159/0004857741104-1118.

- 16 Marshall CB, Shankland SJ: Cell cycle regulatory proteins in podocyte health and disease. *Nephron Exp Nephrol* 2007;106:e51-59.
- 17 Hua W, Huang HZ, Tan LT, Wan JM, Gui HB, Zhao L, Ruan XZ, Chen XM, Du XG: CD36 Mediated Fatty Acid-Induced Podocyte Apoptosis via Oxidative Stress. *PLoS One* 2015;10:e0127507.
- 18 Jiang XS, Chen XM, Wan JM, Gui HB, Ruan XZ, Du XG: Autophagy Protects against Palmitic Acid-Induced Apoptosis in Podocytes *in vitro*. *Sci Rep* 2017;7:42764.
- 19 Green DR, Llambi F: Cell Death Signaling. *Cold Spring Harb Perspect Biol* 2015. DOI: 10.1101/cshperspect.a006080.
- 20 Tummers B, Green DR: Caspase-8: regulating life and death. *Immunol Rev* 2017;277:76-89.
- 21 Eum KH, Lee M: Crosstalk between autophagy and apoptosis in the regulation of paclitaxel-induced cell death in v-Ha-ras-transformed fibroblasts. *Mol Cell Biochem* 2011;348:61-68.
- 22 Huang Y, Dong F, Du Q, Zhang H, Luo X, Song X, Zhao X, Zhang W, Tong D: Swainsonine induces apoptosis through mitochondrial pathway and caspase activation in goat trophoblasts. *Int J Biol Sci* 2014;10:789-797.
- 23 Cory S, Huang DC, Adams JM: The Bcl-2 family: roles in cell survival and oncogenesis. *Oncogene* 2003;22:8590-8607.
- 24 Wu M, Zhang H, Hu J, Weng Z, Li C, Li H, Zhao Y, Mei X, Ren F, Li L: Isoalantolactone inhibits UM-SCC-10A cell growth via cell cycle arrest and apoptosis induction. *PLoS One* 2013;8:e76000.
- 25 Li J, Yuan J: Caspases in apoptosis and beyond. *Oncogene* 2008;27:6194-6206.
- 26 Kantari C, Walczak H: Caspase-8 and bid: caught in the act between death receptors and mitochondria. *Biochim Biophys Acta* 2011;1813:558-563.
- 27 Cao W, Li M, Wu T, Feng F, Feng T, Xu Y, Sun C: alphaMSH prevents ROS-induced apoptosis by inhibiting Foxo1/mTORC2 in mice adipose tissue. *Oncotarget* 2017;8:40872-40884.
- 28 Youle RJ, van der Bliek AM: Mitochondrial fission, fusion, and stress. *Science* 2012;337:1062-1065.
- 29 Chatterjee S, Kundu S, Bhattacharyya A: Mechanism of cadmium induced apoptosis in the immunocyte. *Toxicol Lett* 2008;177:83-89.
- 30 Kumar S, Kain V, Sitasawad SL: High glucose-induced Ca²⁺ overload and oxidative stress contribute to apoptosis of cardiac cells through mitochondrial dependent and independent pathways. *Biochim Biophys Acta* 2012;1820:907-920.
- 31 Sharma V, Anderson D, Dhawan A: Zinc oxide nanoparticles induce oxidative DNA damage and ROS-triggered mitochondria mediated apoptosis in human liver cells (HepG2). *Apoptosis* 2012;17:852-870.
- 32 Chen M, Zhou B, Zhong P, Rajamanickam V, Dai X, Karvannan K, Zhou H, Zhang X, Liang G: Increased Intracellular Reactive Oxygen Species Mediates the Anti-Cancer Effects of WZ35 via Activating Mitochondrial Apoptosis Pathway in Prostate Cancer Cells. *Prostate* 2017;77:489-504.
- 33 Dimmitt SB, Martin JH: Lipid and other management to improve arterial disease and survival in end stage renal disease. *Expert Opin Pharmacother* 2017;18:343-349.
- 34 Liang S, Jin J, Lin B, Gong J, Li Y, He Q: Rapamycin Induces Autophagy and Reduces the Apoptosis of Podocytes Under a Stimulated Condition of Immunoglobulin A Nephropathy. *Kidney Blood Press Res* 2017;42:177-187.
- 35 Piwkowska A: Role of Protein Kinase G and Reactive Oxygen Species in the Regulation of Podocyte Function in Health and Disease. *J Cell Physiol* 2017;232:691-697.
- 36 Gu J, Yang M, Qi N, Mei S, Chen J, Song S, Jing Y, Chen M, He L, Sun L, Hu H, Li L, Wuthrich RP, Wu M, Mei C: Olmesartan Prevents Microalbuminuria in db/db Diabetic Mice Through Inhibition of Angiotensin II/p38/SIRT1-Induced Podocyte Apoptosis. *Kidney Blood Press Res* 2016;41:848-864.
- 37 Xu S, Nam SM, Kim JH, Das R, Choi SK, Nguyen TT, Quan X, Choi SJ, Chung CH, Lee EY, Lee IK, Wiederkehr A, Wollheim CB, Cha SK, Park KS: Palmitate induces ER calcium depletion and apoptosis in mouse podocytes subsequent to mitochondrial oxidative stress. *Cell Death Dis* 2015;6:e1976.
- 38 Yuan Z, Cao A, Liu H, Guo H, Zang Y, Wang Y, Wang Y, Wang H, Yin P, Peng W: Calcium Uptake via Mitochondrial Uniporter Contributes to Palmitic Acid-Induced Apoptosis in Mouse Podocytes. *J Cell Biochem* 2017. DOI: 10.1002/jcb.25930.
- 39 Sieber J, Lindenmeyer MT, Kampe K, Campbell KN, Cohen CD, Hopfer H, Mundel P, Jehle AW: Regulation of podocyte survival and endoplasmic reticulum stress by fatty acids. *Am J Physiol Renal Physiol* 2010;299:F821-829.

- 40 Tao JL, Wen YB, Shi BY, Zhang H, Ruan XZ, Li H, Li XM, Dong WJ, Li XW: Endoplasmic reticulum stress is involved in podocyte apoptosis induced by saturated fatty acid palmitate. *Chin Med J (Engl)* 2012;125:3137-3142.
- 41 Tao JL, Wen YB, Shi BY, Zhang H, Ruan XZ, Li H, Li XM, Dong WJ, Li XW: Endoplasmic reticulum stress is involved in podocyte apoptosis induced by saturated fatty acid palmitate. *Chin Med J* 2012;125:3137-3142.
- 42 Meier P, Vousden KH: Lucifer's labyrinth--ten years of path finding in cell death. *Mol Cell* 2007;28:746-754.
- 43 Ouyang L, Shi Z, Zhao S, Wang FT, Zhou TT, Liu B, Bao JK: Programmed cell death pathways in cancer: a review of apoptosis, autophagy and programmed necrosis. *Cell Prolif* 2012;45:487-498.
- 44 Elmore S: Apoptosis: a review of programmed cell death. *Toxicol Pathol* 2007;35:495-516.
- 45 Repnik U, Stoka V, Turk V, Turk B: Lysosomes and lysosomal cathepsins in cell death. *Biochim Biophys Acta* 2012;1824:22-33.
- 46 Ghobrial IM, Witzig TE, Adjei AA: Targeting apoptosis pathways in cancer therapy. *CA Cancer J Clin* 2005;55:178-194.
- 47 Circu ML, Aw TY: Reactive oxygen species, cellular redox systems, and apoptosis. *Free Radic Biol Med* 2010;48:749-762.
- 48 Thornberry NA, Lazebnik Y: Caspases: enemies within. *Science* 1998;281:1312-1316.
- 49 Prieto-Bermejo R, Hernandez-Hernandez A: The Importance of NADPH Oxidases and Redox Signaling in Angiogenesis. *Antioxidants (Basel)* 2017. DOI: 10.3390/antiox6020032.
- 50 Perry G, Raina AK, Nunomura A, Wataya T, Sayre LM, Smith MA: How important is oxidative damage? Lessons from Alzheimer's disease. *Free Radic Biol Med* 2000;28:831-834.
- 51 Wang W, Cai J, Tang S, Zhang Y, Gao X, Xie L, Mou Z, Wu Y, Wang L, Zhang J: Sinomenine Attenuates Angiotensin II-Induced Autophagy via Inhibition of P47-Phox Translocation to the Membrane and Influences Reactive Oxygen Species Generation in Podocytes. *Kidney Blood Press Res* 2016;41:158-167.
- 52 Mammucari C, Rizzuto R: Signaling pathways in mitochondrial dysfunction and aging. *Mech Ageing Dev* 2010;131:536-543.